Article

CE-ViSNet: An Equivariant Geometric Deep Learning Molecular Force Field with Explicit Chirality Representation

Tao Luo[1,*]

[1] Guizhou University of Finance and Economics, Guiyang, China
* Correspondence: Tao Luo, Guizhou University of Finance and Economics, Guiyang, China

Abstract: The molecular equivariant graph neural network ViSNet is a state-of-the-art model in molecular geometric deep learning. However, because it extracts mirror-invariant geometric features solely through vector dot products, it faces challenges in distinguishing enantiomers, presenting clear limitations in chiral molecular simulation scenarios. To address this limitation, this paper proposes CE-ViSNet (Chiral Enhanced ViSNet), which constructs pseudoscalar chiral features based on the scalar triple product of nearest-neighbor atomic triplets and integrates them into the initial node embeddings without altering the core message-passing architecture. Evaluations on the MD17 and MD22 benchmark datasets demonstrate that CE-ViSNet achieves energy and force prediction accuracy comparable to the original ViSNet. Furthermore, in the chiral mirror-molecule recognition task on the QM9-OR dataset, its classification accuracy rises significantly from 48.89% to 81.20%. By retaining ViSNet's linear computational efficiency, this approach provides a lightweight machine learning force field for molecular dynamics simulations of chiral organic molecules.

Keywords: ViSNet; CE-ViSNet; Equivariant graph neural networks; Chiral molecules; Molecular force fields

1. Introduction

In recent years, machine learning force fields (MLFFs) and deep learning-based molecular representation models have fundamentally reshaped the landscape of atomistic simulations [1]. Across fields such as chemistry, materials science, and biomedicine, molecular dynamics (MD) simulations serve as an indispensable tool for probing microscopic reaction mechanisms and thermodynamic properties. Although first-principles density functional theory (DFT) can provide high-precision molecular energies and atomic forces, its computational cost typically scales steeply with the number of electrons in the system, severely limiting its practical deployment in large-scale, long-timescale simulations such as protein folding, phase transitions, and complex material evolution [2]. To break through this computational bottleneck, equivariant graph neural networks (EGNNs) based on geometric deep learning explicitly incorporate 3D spatial symmetry priors-such as translational and rotational equivariance under $SE(3)$ -enabling the training of quantum-chemically accurate MLFFs using only a small amount of DFT-labeled data. This drastically reduces simulation costs, establishing EGNNs as a mainstream alternative to first-principles calculations. Currently, mainstream EGNNs can be broadly categorized into two technical paradigms:

(1) Lightweight vector-based networks: Exemplified by E2GNN, GemNet, and ViSNet, these models center around first-order directional vector features, relying on vector dot products and orthogonal projections to implicitly extract geometric features such as bond angles, dihedral angles, and improper angles [3-5]. By bypassing the heavy computational and memory burdens associated with Clebsch-Gordan (CG) tensor products, this paradigm achieves linear time complexity $O(N)$ and fast inference speeds,

Received: 15 June 2026
Revised: 30 July 2026
Accepted: 12 August 2026
Published: 17 August 2026

making it exceptionally suited for high-throughput molecular screening and long-timescale MD trajectory evolution.

(2) High-order tensor-based networks: Represented by NequIP, MACE, and Allegro, these models draw upon group representation theory, employing higher-order spherical harmonics tensors coupled with CG products to comprehensively model complex multi-body geometric interactions [2,6,7]. Although offering a higher accuracy ceiling, the parameter sizes, floating-point operation counts, and inference latencies of these models increase significantly with higher tensor degrees, accompanied by massive memory footprints, rendering them difficult to scale to long-timescale simulations of large-scale biomolecules such as peptides and proteins.

As a recently proposed high-performance lightweight equivariant network, ViSNet innovatively introduces a Runtime Geometric Calculation (RGC) module and a Vector-Scalar Interactive Message Passing (ViS-MP) mechanism. It has demonstrated outstanding energy and force prediction accuracy across benchmark datasets such as MD17, MD22, and QM9, while maintaining exceptionally low computational overhead [8-10]. However, the original ViSNet suffers from a fundamental flaw in geometric representation: its RGC module relies entirely on vector dot products to extract geometric features. In 3D geometry and quantitative chirality characterization, chirality is defined as the geometric property of an object being non-superimposable on its mirror image. Because vector dot products are strictly mirror-invariant parity-even scalars, the inner product of two vectors preserves both magnitude and sign under coordinate reflection operations. Consequently, the node and graph-level embedding vectors generated by the network for a molecule and its mirror-image enantiomer are mathematically identical, leaving the model incapable in principle of distinguishing stereoconfigurations of chiral molecules. Chirality is a central physicochemical property of drugs, amino acids, and organocatalytic molecules, with enantiomers frequently exhibiting profound differences in biological activity, metabolic pathways, pharmacological efficacy, and toxicity [11]. As a result, the performance of the original ViSNet degrades significantly when predicting the energies and conformations of chiral systems, failing to meet the rigorous demands of modern stereochemical simulations. Although higher-order tensor models can theoretically encode chiral information through high-order tensor couplings, their prohibitive computational overhead severely restricts their practical utility.

To address the dual challenge of lightweight equivariant networks lacking chiral discrimination and high-order tensor models incurring excessive computational costs, this paper proposes CE-ViSNet (Chiral Enhanced ViSNet), which integrates a plug-and-play Explicit Chirality Module into the embedding layer of the original ViSNet architecture. Inspired by quantitative molecular chirality measures that utilize scalar triple products to characterize spatial chiral orientations, this module constructs pseudoscalar chiral features by calculating the scalar triple product of nearest-neighbor atomic triplet vectors. Algebraically, the scalar triple product quantifies the signed volume of the parallelepiped spanned by three vectors in 3D space; under mirror reflection, its magnitude remains unchanged while its sign undergoes a strict reversal, thus inherently possessing the algebraic capability to discriminate between left- and right-handed enantiomeric configurations. Furthermore, the module leaves the core ViS-MP message-passing logic and linear computational framework of ViSNet intact, merging chiral information into the initial node representations via residual fusion. Evaluations on the MD17 and MD22 molecular dynamics datasets demonstrate that CE-ViSNet achieves energy and force prediction errors on par with the original ViSNet without sacrificing its inherent computational efficiency; in the chiral mirror-molecule recognition task on the QM9-OR dataset, the model's classification accuracy dramatically rises from 48.89% (original ViSNet) to 81.20% [12].

2. Related Works

Lightweight $SE(3)$ equivariant networks center around first-order vector features, eschewing higher-order tensors and CG products to extract molecular angular

information purely through low-dimensional vector operations, thereby achieving lower computational complexity. Early message-passing models such as SchNet and DimeNet utilize only scalar radial distance features or two-body spherical Bessel functions, lacking complete 3D directional and spatial torsional information, which results in weak angular modeling capability for complex topologies [13,14]. PaiNN introduces first-order directional vectors to implicitly encode bond angles via vector dot products, but fails to fully model complex multi-body interactions such as dihedral and improper angles [15]. GemNet explicitly enumerates atomic triplets and quadruplets to extract torsional angles, escalating the computational complexity to $O(N^3)$ and drastically reducing inference speed [4]. ViSNet innovatively introduces the Runtime Geometric Calculation (RGC) framework, which simultaneously models bond angles, dihedral angles, and improper angles with $O(N)$ linear complexity using only vector summation, orthogonal projection, and dot product operations [5]. This is paired with a Vector-Scalar Interactive Message Passing (ViS-MP) mechanism to synchronously update node scalars, node vectors, and edge features. However, from the perspective of spatial symmetry and quantitative chirality theory, the original RGC framework relies entirely on mirror-invariant dot products and lacks pseudoscalar geometric terms possessing parity-odd properties, rendering it fundamentally incapable of capturing mirror symmetry breaking or distinguishing molecular mirror stereostructures.

On the other hand, high-order tensor networks such as NequIP, MACE, and Allegro draw upon group representation theory, employing multi-order spherical harmonics tensors coupled with Clebsch-Gordan tensor products to model multi-body atomic interactions [2,6,7]. Because higher-order spherical harmonics tensors can generate pseudoscalars when coupling odd-degree tensor components, these models theoretically possess chiral discrimination capabilities. Among them, NequIP enhances sample efficiency through multi-layer higher-order tensor interactions, but CG product operations introduce immense floating-point operations and memory bandwidth overhead. MACE optimizes the message-passing architecture to achieve exceptionally high accuracy with as few as two interaction layers; nevertheless, its tensor coupling operations still incur substantial GPU memory footprint and computational latency during both training and inference, posing severe challenges when scaling to long-timescale simulations of biomolecules with hundreds of atoms or more. Although such higher-order tensor models are capable of representing chiral stereostructures, their prohibitive computational costs hinder practical deployment in engineering workflows. Therefore, drawing upon the lightweight principles of pseudoscalar construction from quantitative chirality characterization to develop lightweight solutions that balance efficient inference with chiral discrimination capability holds significant academic value and engineering prospects.

3. CE-ViSNet Model Architecture

CE-ViSNet is constructed upon the original ViSNet equivariant graph neural network framework. Without modifying the core Vector-Scalar Interactive Message Passing (ViS-MP) architecture of ViSNet, a plug-and-play Explicit Chirality Module is introduced into the embedding layer. This module incorporates parity-odd pseudoscalar geometric features via the scalar triple product of nearest-neighbor atomic triplets, overcoming the limitation of the original model in distinguishing chiral enantiomers (As shown in Figure 1).

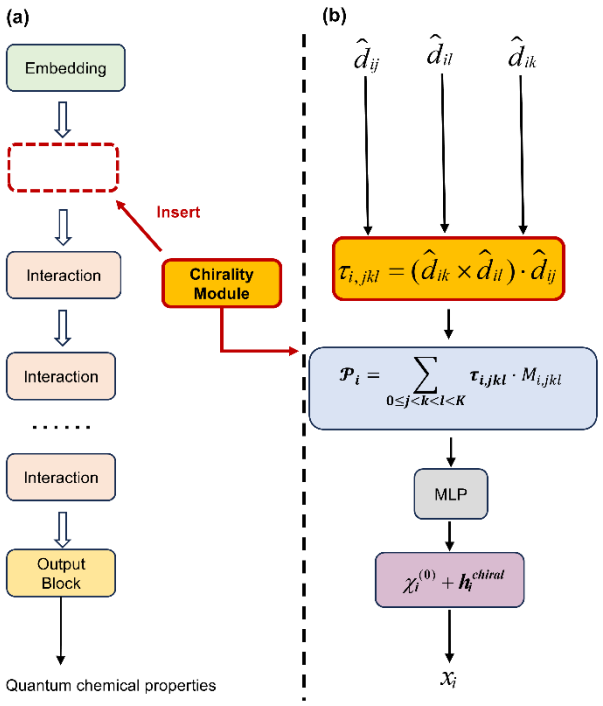

Figure 1. Architecture and Workflow of the Integrated Explicit Chirality Module. (A) Overall Workflow of ViSNet and the Integration Location of the Explicit Chirality Module within the Architecture. (B) Internal Workflow of the Proposed Explicit Chirality Module.

Explicit Chirality Module: Scalar distances and vector dot products exhibit inherent symmetry under mirror reflection operations (i.e., improper rotations $O(3)\backslash SO(3)$), rendering the network incapable of effectively distinguishing enantiomers. The Explicit Chirality Module designed in this study completely decouples distance magnitude information, constructing a node-level chiral pseudoscalar using solely the scalar triple product of adjacent unit directional vectors.

3.1. Deterministic Neighborhood Selection and Triplet Construction

For a target node i in the molecular graph, the unit directional vector pointing toward its neighbor node $j \in N(i)$ is defined as:

$$\hat{\mathbf{d}}_{ij} = \frac{\mathbf{P}_j - \mathbf{P}_i}{\|\mathbf{P}_j - \mathbf{P}_i\|_2} \quad (1)$$

Where $\mathbf{P}_i \in R^3$ denotes the 3D spatial coordinates of node i .To eliminate ambiguity in triplet combinations caused by graph data storage ordering while maintaining the determinism of feature computation, the module constructs a globally unique sorting key using the relative distance $r_{ij} = \|\mathbf{P}_j - \mathbf{P}_i\|_2$:

$$\text{Key}_{ij} = i \times 10^7 + r_{ij} \quad (2)$$

Based on Key_{ij} , the neighbors of node i are sorted in ascending order, and the nearest K neighbors are selected (setting a truncation limit K=max_neighbors , with a default of K=8). Within this ordered neighborhood, all unique triplet index combinations (j,k,l) satisfying $0 \le j < k < l < K$ are extracted.

3.2. Pure Geometric Scalar Triple Product and Pseudoscalar Representation

For any triplet (j,k,l) constructed from the first K neighbors, the corresponding unit directional vectors $\hat{\mathbf{d}}_{ij}, \hat{\mathbf{d}}_{ik}, \hat{\mathbf{d}}_{il} \in R^3$ are extracted. The spatial stereochirality of this triplet is computed via the scalar triple product of the three vectors:

$$\tau_{i,jkl} = \hat{\mathbf{d}}_{ij} \cdot (\hat{\mathbf{d}}_{ik} \times \hat{\mathbf{d}}_{il}) \quad (3)$$

Geometrically, $\tau_{i,jkl}$ is equivalent to the signed volume of the parallelepiped spanned by these three unit directional vectors. Because only unit directional vectors are used, this calculation completely eliminates the influence of interatomic distance magnitudes

r_{ij}, r_{ik}, r_{il} , achieving complete decoupling between chiral topology and distance information.

3.3. Symmetry and Chiral-Sensing Algebraic Properties

Intrinsic Rotation Invariance: For any rigid-body rotation matrix $\mathbf{R} \in SO(3)$, since $\det(\mathbf{R}) = 1$, we have:

$$\tau_{i,jkl}' = (\mathrm{R}\hat{\mathrm{d}}_{ij}) \cdot \left((\mathrm{R}\hat{\mathrm{d}}_{ik}) \times (\mathrm{R}\hat{\mathrm{d}}_{il}) \right) = \det(\mathrm{R})\ \tau_{i,jkl} = \tau_{i,jkl} \quad (4)$$

Mirror Reflection Parity (Chiral Sensing): For any mirror reflection matrix $\mathrm{M} \in O(3) \setminus SO(3)$, since $\det(\mathrm{M}) = -1$, we have:

$$\tau_{i,jkl}' = \det(\mathrm{M})\ \tau_{i,jkl} = -\tau_{i,jkl} \quad (5)$$

This indicates that $\tau_{i,jkl}$ is a canonical geometric pseudoscalar. When the molecular structure undergoes mirror reflection, the sign of $\tau_{i,jkl}$ strictly reverses ($\tau \to -\tau$), providing a direct algebraic criterion for the neural network to discriminate enantiomers.

3.4. Mask Aggregation and Feature Injection

To eliminate interference from invalid neighbors caused by dense matrix padding, the module introduces a joint triplet validity mask $M_{i,jkl}$:

$$M_{i,jkl} = m_{ij} \wedge m_{ik} \wedge m_{il} \quad (6)$$

where $m_{ij} \in \{0,1\}$ indicates whether node j is a valid neighbor of node i .Summing all valid triplet pseudoscalars associated with target node i yields the node-level explicit chirality score $\mathrm{P}_i \in \mathrm{R}^1$:

$$\mathrm{P}_i = \sum_{0 \le j < k < l < K} \tau_{i,jkl} \cdot M_{i,jkl} \quad (7)$$

If target node i has fewer than three valid neighbors (i.e., $K < 3$), P_i is directly set to 0 .Finally, a lightweight Multi-Layer Perceptron (MLP) maps the one-dimensional pseudoscalar P_i into the hidden feature dimension d (d=hidden_channels):

$$\mathrm{h}_i^{\mathrm{chiral}} = \mathrm{MLP}(\mathrm{P}_i) = \mathrm{W}_2 \cdot \mathrm{SiLU}(\mathrm{W}_1 \mathrm{P}_i + \mathrm{b}_1) + \mathrm{b}_2 \quad (8)$$

where the transformation weight matrices are $\mathbf{W}_1 \in \mathrm{R}^{(d/2) \times 1}$ and $\mathbf{W}_2 \in \mathrm{R}^{d \times (d/2)}$, respectively.

The generated chiral feature vector $\mathrm{h}_i^{\mathrm{chiral}}$ is directly injected into the initial node embedding feature $\mathbf{x}_i^{(0)}$ via a residual connection:

$$\mathbf{x}_i \leftarrow \mathbf{x}_i^{(0)} + \mathbf{h}_i^{\mathrm{chiral}} \quad (9)$$

The node representation $\mathbf{x}_i$, now enriched with chiral awareness, serves as the primary input for the subsequent ViS-MP message-passing network, granting the entire network the capacity to perceive local spatial chirality.

4. Experimental Analysis

4.1. Experimental Details

The chiral dataset (QM9-OR) was randomly partitioned into training, validation, and test sets according to a 7:1.5:1.5 ratio. Following standard practices in prior relevant studies, we filtered the dataset to include only molecules containing a single chiral center, thereby avoiding potential confounding effects caused by interactions between multiple chiral centers during model learning. For the achiral datasets (MD17 and MD22), the data partitioning strictly followed the original setup of ViSNet. All baseline methods and our model were trained and evaluated under identical data splits and evaluation protocols to ensure fair and rigorous comparability.

4.2. QM9-OR Enantiomer Recognition Experiment

To verify the effectiveness of the Explicit Chirality Module in overcoming the "chiral blind spot" of traditional equivariant models, we performed Principal Component Analysis (PCA) visualization on the high-dimensional latent feature representations learned by the models. In the experiment, corresponding mirror-image molecular pairs were generated via strict spatial inversion of 3D molecular coordinates to evaluate the model's binary classification capability in distinguishing these two enantiomeric classes.

As shown in Figure 2, the experimental results indicate that, constrained by strict mirror symmetry, the original ViSNet baseline model completely fails in the enantiomer

recognition task. Because it cannot perceive mirror transformations, the latent features of the original and mirror-image configurations severely overlap in the PCA-reduced space, yielding a classification accuracy of only 48.89% (equivalent to random guessing).

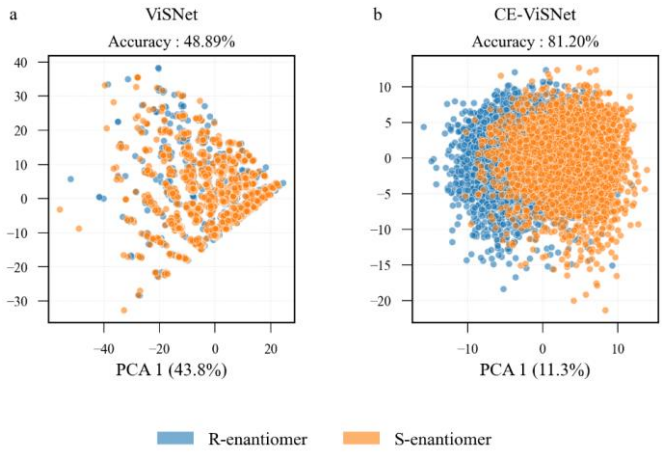

Figure 2. Principal Component Analysis (PCA) Visualization of Latent Feature Representations Across Models in the Enantiomer Recognition Task. (A) Dimensionally Reduced Distribution of Features Extracted by the Original ViSNet Model for Mirror-Image (R) -Configurations (Blue) and (S) -Configurations (Orange), Along with Its Corresponding Classification Accuracy. (B) Dimensionally Reduced Distribution of Features and Classification Accuracy Extracted by the Chiral-Enhanced Model CE-ViSNet for the Same Set of Mirror-Image Molecules.

In contrast, after integrating the Explicit Chirality Module, the chiral discrimination performance of CE-ViSNet improves significantly, with the chiral mirror-molecule classification accuracy surging to 81.20%. This result strongly demonstrates that the proposed module successfully guides the model to explicitly and accurately encode chirality-related geometric differences within the deep feature space.

4.3. Physical Force Field Prediction Experiments on MD17 and MD22

To further evaluate the impact of the Explicit Chirality Module on the model's general physical property prediction performance, we conducted molecular energy and atomic force prediction benchmarks across 14 molecular systems from the MD17 and MD22 datasets.

The experimental results are presented in Table 1 and Table 2. The evaluation demonstrates that while the Explicit Chirality Module significantly enhances the model's chiral perception capability, it incurs no loss in the prediction accuracy of energy and forces compared to the baseline model. CE-ViSNet achieves prediction errors comparable to those of the original ViSNet across both datasets. This indicates that the introduced chiral mechanism increases parity sensitivity without compromising the model's ability to correctly model translational and rotational symmetries, thereby preserving strict physical consistency in force field predictions.

Table 1. Mean Absolute Errors (MAE) of Energies (Kcal Mol) and Forces (Kcal Mol Å) for 7 Small Organic Molecules in MD17

Model	Aspirin		Ethanol		Malondialdehyde		Naphthalene		Salicylic acid		Toluene		Uracil	
	Energy	Forces	Energy	Forces	Energy	Forces	Energy	Forces	Energy	Forces	Energy	Forces	Energy	Forces
Visnet	0.116	0.155	0.051	0.060	0.075	0.100	0.085	0.039	0.092	0.084	0.074	0.039	0.095	0.062

CE-Visnet	0.119	0.159	0.055	0.063	0.080	0.098	0.080	0.041	0.096	0.086	0.071	0.042	0.094	0.060

Table 2. Mean Absolute Errors (MAE) of Energy (Kcal/mol) and Force (kcal/mol/Å) for 7 Large-Scale Molecules on MD22

Model	**Ac-Ala3-NHMe**		**AT-AT**		**AT-AT-CG-CG**		**DHA**		**Buckyball catcher**		**Stachyose**		**Double-walled nanotube**	
	Energy	Forces	Energy	Forces	Energy	Forces	Energy	Forces	Energy	Forces	Energy	Forces	Energy	Forces
Visnet	0.064	0.083	0.071	0.081	0.196	0.148	0.074	0.060	0.508	0.184	0.092	0.088	0.800	0.362
CE-Visnet	0.066	0.090	0.071	0.079	0.201	0.144	0.078	0.061	0.509	0.199	0.100	0.085	0.790	0.355

5. Conclusion

To address the inability of the original ViSNet to distinguish molecular 3D chiral enantiomers, this paper proposes CE-ViSNet, a chiral-enhanced molecular geometric deep learning force field. The model introduces a purely geometric Explicit Chirality Module that constructs pseudoscalar chiral features via scalar triple products of nearest-neighbor atomic triplets, overcoming the chiral representation limitation while fully preserving the original network's linearly efficient message-passing architecture. Benchmark evaluations on the MD17 and MD22 datasets show that CE-ViSNet achieves energy and force prediction accuracy on par with the baseline, while its accuracy in chiral mirror-molecule recognition on the QM9-OR dataset surges significantly from 48.89% to 81.20%. This lightweight scheme successfully balances computational efficiency with stereochemical representation capability, rendering it exceptionally well-suited for molecular dynamics simulations of chiral small molecules and peptide systems. Future work could explore dynamically embedding stereochiral features into each message-passing layer to further enhance stereoscopic modeling performance for ultra-large biomacromolecules.

Funding: This research received no external funding.

Conflicts of Interest: The authors declare no conflict of interest.

Acknowledgments: The authors acknowledge Guizhou University of Finance and Economics for providing computational facilities and academic support.

References

1. O. T. Unke, S. Chmiela, H. E. Sauceda, et al., "Machine learning force fields," *Chemical Reviews*, vol. 121, no. 16, pp. 10142–10186, 2021.
2. S. Batzner, A. Musaelian, L. Sun, et al., "E(3)-equivariant graph neural networks for data-efficient and accurate interatomic potentials," *Nature Communications*, vol. 13, no. 1, p. 2453, 2022.
3. Z. Yang, X. Wang, Y. Li, et al., "Efficient equivariant model for machine learning interatomic potentials," *npj Computational Materials*, vol. 11, no. 1, p. 49, 2025.
4. J. Gasteiger, F. Becker, and S. Günnemann, "GemNet: Universal directional graph neural networks for molecules," in *Advances in Neural Information Processing Systems*, vol. 34, pp. 6790–6802, 2021.
5. Y. Wang, T. Wang, S. Li, et al., "Enhancing geometric representations for molecules with equivariant vector-scalar interactive message passing," *Nature Communications*, vol. 15, no. 1, p. 313, 2024.
6. I. Batatia, D. P. Kovacs, G. Simm, et al., "MACE: Higher order equivariant message passing neural networks for fast and accurate force fields," in *Advances in Neural Information Processing Systems*, vol. 35, pp. 11423–11436, 2022.
7. A. Musaelian, S. Batzner, A. Johansson, et al., "Learning local equivariant representations for large-scale atomistic dynamics," *Nature Communications*, vol. 14, no. 1, p. 579, 2023.

8. K. T. Schütt, F. Arbabzadah, S. Chmiela, et al., "Quantum-chemical insights from deep tensor neural networks," *Nature Communications*, vol. 8, no. 1, p. 13890, 2017.
9. S. Chmiela, V. Vassilev-Galindo, O. T. Unke, et al., "Accurate global machine learning force fields for molecules with hundreds of atoms," *Science Advances*, vol. 9, no. 2, p. eadf0873, 2023.
10. R. Ramakrishnan, P. O. Dral, M. Rupp, et al., "Quantum chemistry structures and properties of 134 kilo molecules," *Scientific Data*, vol. 1, no. 1, p. 140022, 2014.
11. M. Sparta, C. Riplinger, and F. Neese, "Mechanism of olefin asymmetric hydrogenation catalyzed by iridium phosphino-oxazoline: a pair natural orbital coupled cluster study," *Journal of Chemical Theory and Computation*, vol. 10, no. 3, pp. 1099–1108, 2014.
12. Y. Zhou, H. Zhu, Y. Yuan, et al., "Machine learning classification of chirality and optical rotation using a simple one-hot encoded cartesian coordinate molecular representation," *Journal of Chemical Information and Modeling*, vol. 65, no. 9, p. 4281, 2025.
13. K. T. Schütt, H. E. Sauceda, P. J. Kindermans, et al., "SchNet—a deep learning architecture for molecules and materials," *The Journal of Chemical Physics*, vol. 148, no. 24, p. 241722, 2018.
14. J. Gasteiger, J. Groß, and S. Günnemann, "Directional message passing for molecular graphs," *arXiv preprint arXiv:2003.03123*, 2020.
15. K. Schütt, O. Unke, and M. Gastegger, "Equivariant message passing for the prediction of tensorial properties and molecular spectra," in *International Conference on Machine Learning*, PMLR, pp. 9377–9388, 2021.